Investigation of carrier transport and carrier distribution in GaAs/(Al,Ga)As quantum-cascade structures

T. Ohtsuka, L. Schrottke, R. Hey, H. Kostial, and H. T. Grahn[a)]
Paul-Drude-Institut für Festkörperelektronik, Hausvogteiplatz 5-7, 10117 Berlin, Germany

(Received 13 May 2003; accepted 23 May 2003)

We have investigated the current density–electric field (*j-F*) characteristics and photoluminescence (PL) spectra of several GaAs/(Al,Ga)As quantum-cascade structures (QCS's) up to the threshold field strength to obtain information on the carrier distribution and field inhomogeneities. Due to the complex structure of each single period of the cascaded device, the dark *j-F* characteristics of undoped QCS's exhibit distinct current maxima, resulting in regions of negative differential conductivity, while a plateaulike feature appears under illumination. For doped QCS's, a plateau with sawtoothlike structures appears, which are well known from doped, weakly coupled superlattices under electric-field-domain formation. However, in contrast to the splitting of the PL line that is observed for doped, weakly coupled superlattices, no splitting has been observed in the doped QCS's. The *j-F* characteristic of an undoped QCS with thicker barriers than the original QCS exhibits a much more pronounced current maximum in the dark. Under illumination, the *j-F* characteristic of this structure shows a clear plateaulike feature, which contains additional fine structure indicating the existence of electric-field inhomogeneities within each period due to the separation of electrons and holes. The PL spectra of the undoped and doped QCS's show emission from only the widest quantum well (QW) because the holes accumulate very quickly in this QW resulting from the strong coupling within the entire QCS. However, in the PL spectra of the undoped QCS with thicker barriers, PL lines from several quantum wells can be identified. The carrier distribution process in QCS's is also discussed as a function of the applied electric field and compared for the different structures. © *2003 American Institute of Physics.*
[DOI: 10.1063/1.1592612]

I. INTRODUCTION

Quantum-cascade lasers (QCL's) are light-emitting devices based on resonant tunneling and intersubband transitions in quantum wells (QW's), and their design results from sophisticated band-structure engineering of quantum structures. Since the report on the successful operation of QCL's by Faist *et al.*,[1] their performance has improved rapidly, and recently room temperature cw operation[2] and terahertz laser emission[3] have been reported. A comprehensive review of earlier developments can be found in Ref. 4. Although a number of QCL's have been realized using the material systems (In,Ga)As/(In,Al)As lattice matched and strain compensated on InP, GaAs/(Al,Ga)As on GaAs, and most recently InAs/AlSb on InAs,[5] there are only a few reports of the experimental investigation of the basic processes of QCL's, such as the subband population.[6] Due to the complex structure of QCL's, detailed experimental studies of the individual underlying processes are difficult to perform, but a recent study[7] of the lasing properties of GaAs/(Al,Ga)As QCL's underlines the necessity of such investigations.

QCL's usually consist of a periodic repetition of two functional regions: an active region and an injector region. The 25–30 periods of these two regions are sandwiched between waveguide and contact layers. The active region is usually formed by two or three quantum wells, while the injectors consist of chirped (graded-gap) superlattices (SL's). For so-called interminiband QCL's, the active region can also be formed by a chirped SL. At the operation field strength, a miniband is formed in the injector region, allowing coherent electron transport into the upper laser level of the active region.[8] The miniband formation in the injector at finite field strengths may be connected with a nonlinear transport behavior such as negative differential conductance (NDC). Sirtori *et al.*[9] reported the observation of NDC for higher field strengths, when the coupling between the injector state and the upper laser level is reduced. Very recently, calculations of the transport properties of GaAs/(Al,Ga)As QCL's showed NDC only for $Al_{0.45}Ga_{0.55}As$ barriers, but not for $Al_{0.33}Ga_{0.67}As$ barriers.[10] Therefore, a detailed understanding of the origin of the NDC may contribute to an improvement of device characteristics such as efficiency and threshold current density.

In this paper, we report an experimental investigation of miniband formation and carrier redistribution in GaAs/(Al,Ga)As QC structures (QCS's), following the design by Sirtori *et al.*,[11] using current density–electric field (*j-F*) characteristics and interband photoluminescence (PL) spectroscopy. The transport characteristics for GaAs/(Al,Ga)As QCS's exhibit plateaulike features, which are similar to structures in the *j-F* characteristics of moderately doped, weakly coupled SL's under electric-field-domain formation.[12] In order to determine the origin of these plateaulike features, we also investigated an undoped QCS, in which

a)Electronic mail: htgrahn@pdi-berlin.de

the cladding layers are replaced by simple n^+-GaAs contact layers, under photoexcitation for different excitation powers. This undoped QCS exhibits a well-defined jump to lower current values at the field strength where the lower laser level is populated.[13]

The detection of the carrier distribution within the injector in GaAs/(Al,Ga)As QCS's by PL spectroscopy is hardly possible, since the optically excited holes quickly relax into the widest QW.[14,15] However, the holes can serve as a probe for those electrons that occupy higher subbands within the active region, so that the field-induced occupation of the laser levels can be investigated. Recently, we directly observed the PL signal from the lower laser level[13] as well as the upper laser level, although much weaker in intensity, in interband PL spectra. In the present work, the carrier distribution is derived by comparing both the *j-F* characteristics and the PL spectra with the corresponding data recorded for a quasi-QCL structure, in which the barriers are considerably thicker than in the original QCL structure.

II. EXPERIMENTAL SETUP

For this investigation, four different GaAs/$Al_{0.33}Ga_{0.67}As$ QCS's grown by molecular-beam epitaxy on n^+-GaAs(100) substrates were used. Based on the design by Sirtori *et al.*,[11] the layer sequence in one period starting from the injection barrier is 5.8, **1.5**, 2.0, **4.9**, 1.7, **4.0**, 3.4, **3.2**, 2.0, **2.8**, 2.3, **2.3**, 2.5, **2.3**, 2.5, **2.1**, where the layer thicknesses are given in nanometers, numbers in boldface refer to GaAs well layers, and underlined numbers denote doped layers for those QCS's with doped injectors. This layer sequence is used for sample A, which contains $N=20$ periods and undoped injectors. At the same time, the cladding layers are replaced by 400 nm n^+-GaAs contact layers. Sample B is also undoped with a layer sequence of 9.6, **1.5**, 4.6, **4.9**, 4.8, **4.0**, 6.9, **3.2**, 4.5, **2.8**, 4.7, **2.3**, 4.9, **2.3**, 4.9, **2.1**. However, compared to sample A, the thickness of the (Al,Ga)As barriers was increased by approximately a factor of 2 in order to decrease the coupling between the wells. The actual barrier thicknesses were determined to achieve a quasiminiband at the threshold voltage similar to the one of sample A. For comparison, we also investigated a sample of the same structure as sample B, but with doped injectors, which is labeled B′. Sample C is a complete QCL structure with the same layer sequence as sample A, but it contains 30 periods, doped injectors, thick cladding layers for waveguiding, and contact layers. The doping density per period was 5.8×10^{11} cm^{-2} for sample B′ and 4.1×10^{11} cm^{-2} for sample C.

The accuracy of the layer sequence was confirmed using x-ray diffractometry and scanning electron microscopy. After growth, the samples were processed into mesa structures and mounted on sapphire plates with sputtered gold stripes. Samples A, B, and B′ were processed into circular mesas of 215 and 425 μm diameter, while sample C was shaped into a rectangular mesa of 40×80 μm^2 area. The current-voltage characteristics were recorded using a current/voltage source (Hewlett-Packard, model 3245A) and a digital multimeter (Hewlett-Packard, model 3458A). For pulsed measurements, a pulse generator (Hewlett-Packard, model 8116A), boxcar integrator (EG&G, model 4121B), and analog-digital converter (EG&G, model 4161A) were used. The current-voltage characteristics under illumination were measured using a Ti:sapphire laser for photoexcitation. For the PL measurements, the QCS's were excited using either a tunable Ti:sapphire or a tunable dye laser pumped by an Ar^+-ion laser, and the diameter of the excitation spot was typically 50 to 100 μm. The luminescence was then detected with a 1 m monochromator and a charge-coupled-device detector. During all of the measurements, the samples were cooled on a cold finger of a He flow cryostat. The applied voltage V_{app} was converted into a field strength by dividing it by the total thickness of the QCS (including a 25 nm spacer layer on either side of the QCS for samples A and B) without any contact or cladding layers.

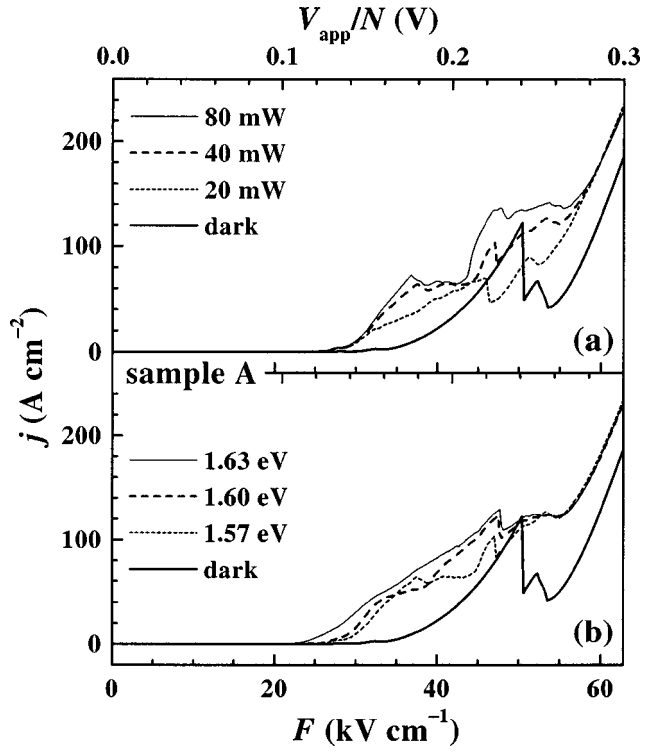

FIG. 1. *j-F* characteristics of sample A (a) in the dark as well as for different light intensities with a photon energy of 1.57 eV and (b) for different photon energies at an intensity of 40 mW. All curves were recorded at a sample temperature $T=5$ K.

III. EXPERIMENTAL RESULTS

A. Undoped quantum-cascade structure

The *j-F* characteristics in the dark and for different light powers at an excitation energy of 1.57 eV (an energy below the band gap of the widest QW) are shown in Fig. 1(a) for the undoped sample A. The characteristic in the dark exhibits a large jump to lower current values near 50 kV cm^{-1}, which corresponds to the field strength of miniband formation in the injector for this sample. When carriers are optically excited with an excitation energy of 1.57 eV, electrons and holes are generated only in the GaAs contact layers, and plateaulike structures appear above 25 kV cm^{-1}. For the highest power presented, two plateau regions appear between

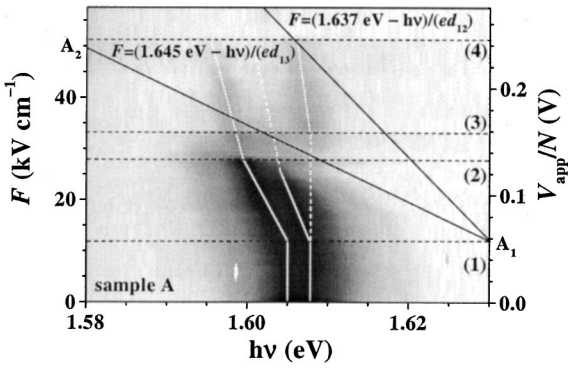

FIG. 2. Gray-scale representation of the logarithm of the PL intensity of sample A versus photon energy $h\nu$ and electric-field strength F recorded at $T=5$ K. The excitation energy was 1.968 eV and the power 0.15 mW. The white lines following the PL peak(s) are guides to the eyes. The black lines indicate the field dependence of the spatially indirect transitions between the electrons in wells 2 and 3 with holes in the widest well 1.

35 and 40 as well as 47 and 55 kV cm^{-1}. Figure 1(b) displays the *j-F* characteristics for different excitation energies at a fixed power of 40 mW. The curves in the dark and for an excitation energy of 1.57 eV are identical to the ones in Fig. 1(a). When the excitation energy becomes 1.63 eV or larger, carriers are also excited in the widest QW of each period of the QCS, resulting in a larger photocurrent for field strengths up to 53 kV cm^{-1}. Therefore, the plateaulike structure can be induced by carriers injected from the contacts as well as by carriers excited within the widest quantum well. The first plateau in the *j-F* characteristic in Fig. 1(b) disappears for excitation at photon energies above 1.57 eV.

PL spectra as a function of electric-field strength are shown in Fig. 2 in a two-dimensional gray-scale representation, where the dark areas correspond to large PL intensities. In sample A, only PL from the widest QW is observed. By increasing F from 11 to 28 kV cm^{-1}, the PL peak shifts to lower energies, and between 35 and 50 kV cm^{-1}, the PL peak splits into two distinct lines for weak excitation. The origin of this peak splitting is possibly the coexistence of excitons and free electron-hole pairs. A diagonal transition between the subband of the widest well and the subband of the other wells can be excluded as a possible cause for the splitting, because the difference in the redshift of the two peaks is too small. This field range coincides approximately with the plateau regions in the photoexcited *j-F* characteristics for 40 and 80 mW excitation power shown in Fig. 1(a).

The peak-splitting feature is not clearly resolved for higher excitation powers. Figure 3 shows several PL spectra of the undoped QCS for small and large excitation powers and different electric-field strengths. Between 0 and 21 kV cm^{-1}, the PL peak exhibits a small splitting. At 42 kV cm^{-1}, the splitting becomes larger and corresponds to the splitting already shown in Fig. 2. In addition, smaller peaks can be observed in between the two distinctive peaks for some field strengths. However, for strong excitation, a central peak located between the two distinctive peaks for weak excitation becomes dominant. Figure 4 demonstrates the correspondence between the integrated PL intensity and the *j-F* characteristics for sample A. The *j-F* characteristic shows

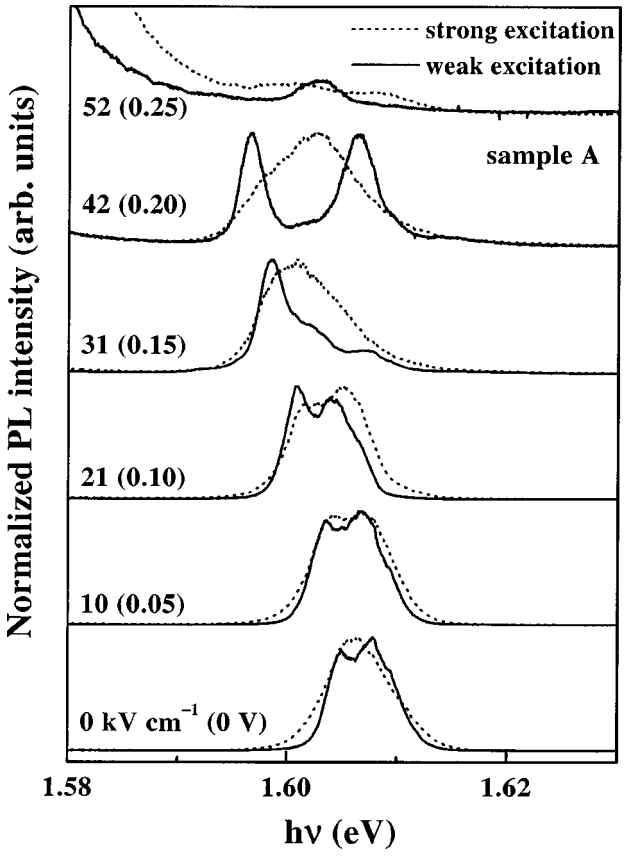

FIG. 3. Comparison of the normalized PL spectra of sample A for weak (0.5 μW) and strong (150 mW) excitation at a photon energy of 1.746 eV for different electric-field strengths (voltages per period) at $T=5$ K.

three jumps at the points 2, 3, and 4, which are correlated with abrupt changes of the PL intensity in Fig. 2.

B. Quasi quantum-cascade structure

In sample B, the weaker coupling due to the thicker barriers leads to a smaller but sharper resonance in the dark current near the expected voltage for miniband formation as

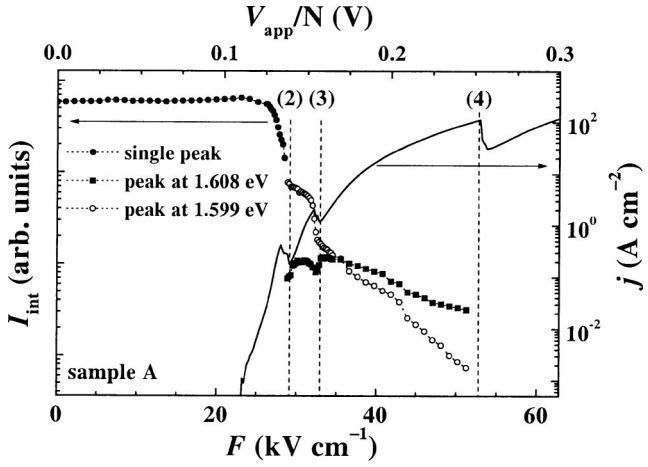

FIG. 4. Comparison between the field dependence of the logarithm of the integrated PL intensity I_{int} from the widest QW and the dark current density j of sample A. The sample is at $T=5$ K and photoexcited at 1.70 eV with a power of 1 μW.

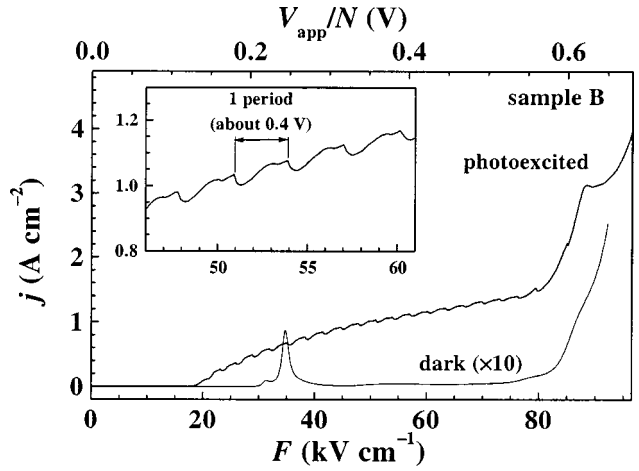

FIG. 5. Dark and photoexcited *j-F* characteristics of sample B for an excitation energy of 1.63 eV, laser power of approximately 50 mW, and temperature $T=5$ K. The inset shows an enlarged section of the photoexcited *j-F* characteristics.

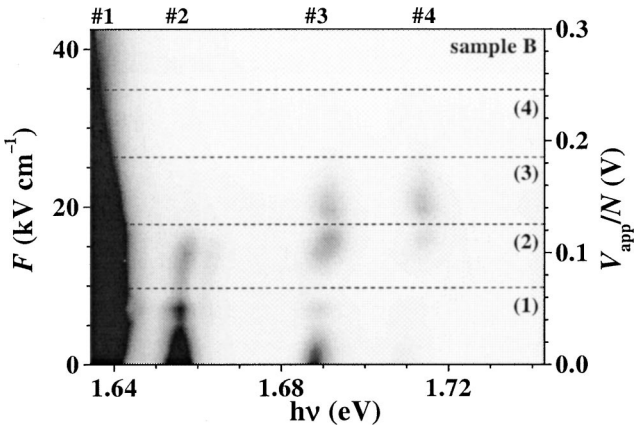

FIG. 6. Gray-scale representation of the PL intensity in sample B versus photon energy $h\nu$ and electric-field strength F for photoexcitation at 1.968 eV with a power of 15 mW recorded at $T=5$ K. The numbers on top identify the different wells.

shown in Fig. 5. In this sample, strong optical excitation with a power of approximately 50 mW and a photon energy of 1.63 eV, which creates carriers in the widest QW but not in the other wells, induces a plateaulike structure in the *j-F* characteristic with a superimposed periodic modulation. The number of periods of this modulation corresponds exactly to the number of periods of this QCS. Therefore, this plateaulike structure can be considered as a signature of an inhomogeneous field distribution, which is typically observed in weakly coupled SL's under electric-field-domain formation. The 0.4 V period of both structures is much larger than the calculated energy level separation of about 0.17 V between the ground state and the upper laser level in the widest QW. If carriers are excited in only the widest QW (1.63 eV) and in the contacts, the modulation contains two peaks in each period as shown in the inset of Fig. 5. However, these small peaks degenerate into one for photoexcitation at higher energies. The substructure of the modulation seems to result from an inhomogeneous distribution of the carriers within each period, since with increasing photon energy carriers are excited in an increasing number of QW's, so that the initial carrier distribution becomes increasingly more homogeneous. The appearance of two structures per period could be due to screening effects within a single stage of the cascade. In this case, the excitation of electrons and holes and their subsequent separation, due to the different subband structure for each type of carrier, may generate internal electric fields within each period. Another possibility for the appearance of two structures per period is the alignment between a confined state in the well and a higher-energy state such as a quasicontinuum state.

For sample B, a well-defined spatial carrier distribution should be observable because of the thicker barriers. Therefore, not only the PL peak from the widest QW (well 1), but several additional peaks from narrower QW's (well 2, 3, and 4) are also observed as shown in Fig. 6. The energy shift of the peak from each well with increasing field is much smaller than in sample A and is probably due to the much weaker interaction between the QW's in sample B. With increasing electric field, the intensity of each peak exhibits a variation, which can be related to a carrier redistribution process. Figure 7 shows the correlation between the field dependence of the logarithm of the PL intensity of the widest QW and the current density j in sample B. From Figs. 6 and 7, at least four characteristic field strengths can be identified, which are essential for the understanding of the carrier redistribution process in this quasi-QCS. The redistribution process for all samples is discussed in Sec. IV.

C. Complete quantum-cascade structure

Figure 8 shows the *j-F* characteristics for sample C recorded at sample temperatures $T=5$ and 77 K for voltage and current control measurements, and a *j-F* characteristic under pulsed operation recorded at 77 K is also included. The designed voltage for miniband formation for this sample is about 48 kV cm^{-1}, and a plateau is observed in the range of 33–48 kV cm^{-1}. Although the observation of this feature was not reported in Refs. 9 and 11, such plateaulike structures have recently been observed in several GaAs/

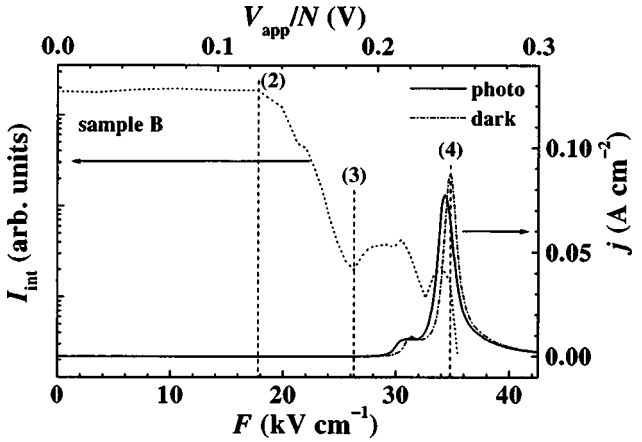

FIG. 7. Comparison between the field dependence of the logarithm of the integrated PL intensity I_{int} from the widest QW detected at approximately 1.628 eV and the current density j of sample B at $T=5$ K. The sample is excited at 1.746 eV with a power of 0.1 μW.

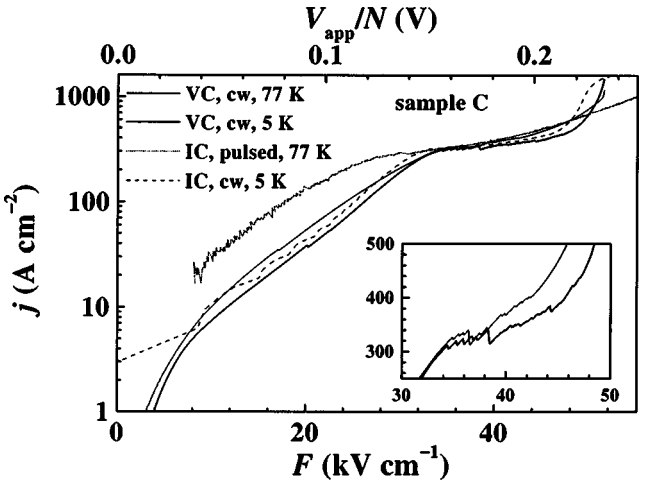

FIG. 8. Logarithm of the current density j versus field strength F of sample C. VC and IC denote voltage- and current-controlled operation, respectively. The pulsed measurement was performed using a frequency of 2 kHz and a duty cycle of 0.2%. The inset shows an enlarged section of the plateau region for the voltage-controlled measurements on a linear scale.

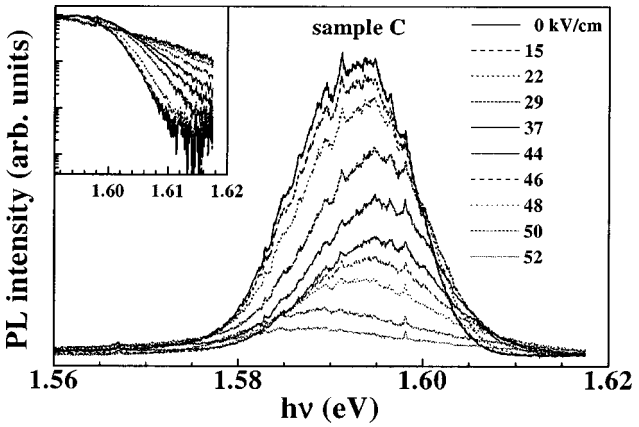

FIG. 9. PL spectra from sample C for various applied electric fields recorded at $T=5$ K. The inset shows the intensity of the high-energy tail of the PL line on a logarithmic scale.

(Al,Ga)As QCL's.[15,16] This plateau appears to be a universal feature, since it is present in both QCL structures that lase as well as in those that do not lase. For voltage-controlled measurements, a sawtooth shaped structure appears on top of the plateau, and, above 48 kV cm^{-1}, the current increases exponentially. The current density in the plateau region has a value of about 0.35 kA cm^{-2}, which is much smaller than the corresponding laser threshold.[7] This plateau is very similar to the one observed in weakly coupled SL's under electric-field-domain formation.[12] However, a splitting of the PL peaks due to different field strengths, which is usually detected in weakly coupled SL's under electric-field-domain formation, is not observed for this sample. The shape of the *j-F* characteristics does not change significantly when the temperature is increased from 5 to 77 K.

Considering the generation of the plateau, two possible origins, not related to the properties of a particular sample, can be excluded. The experimental procedure cannot be the origin, since both the voltage-controlled and the current-controlled measurements, although different in their circuit impedance, result in almost the same shape of the *j-F* characteristics. Sample heating may also be an important factor. However, the *j-F* characteristic under pulsed operation exhibits the same plateaulike feature, although lattice heating should be negligible in this case. Therefore, sample heating can also be excluded as the origin for the generation of the plateau. Thus, the plateau region should originate from the transport properties, which are mainly determined by the structural parameters, i.e., the layer sequence of the QCL structure, and a more detailed discussion of the plateau is given below.

For the PL spectra, the complete QCL structure (sample C) was illuminated from the cleaved edge because of the thick cladding layer on the top. PL lines originating from narrower QW's were not observed. The PL measurements are useful for a qualitative investigation of the subband population of the widest QW, but are not suitable for a direct observation of the spatial carrier distribution in the complete QCL structure.

Figure 9 shows the PL spectra for different applied electric fields recorded at 5 K. As for sample A, the PL spectra exhibit only one line at about 1.593 eV for $V_{app}=0$ V, resulting from recombination of electrons and holes in their respective ground states of the widest QW. With increasing electric field, the peak intensity decreases. At the same time, the peak shifts to higher energies up to $F=44$ kV cm^{-1}, while for $F>46$ kV cm^{-1} the peak energy shift is reversed toward lower energies. An electric-field-induced blueshift has previously been reported for coupled double-quantum-well structures.[17,18] However, we attribute both the blue- and the redshift of the PL peak to an increasing temperature (lattice and/or carrier) due to the increasing current. When the temperature of the sample is changed at zero bias, a very similar peak shift is observed as shown in Fig. 10. In fact, the field dependence of the high-energy tail of the PL line indicates an increasing temperature due to heating by current injection as shown in the inset of Fig. 9. However, it should

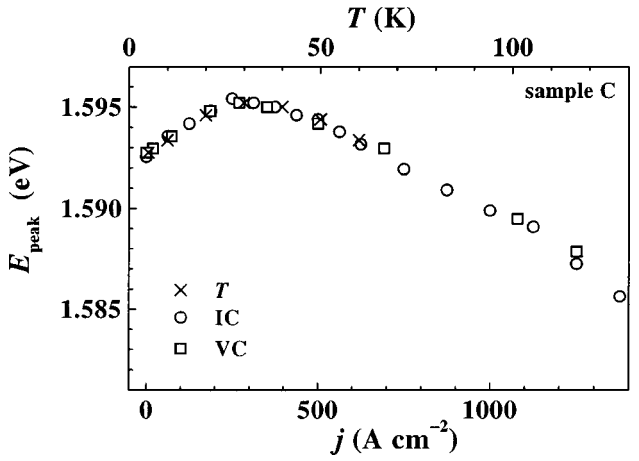

FIG. 10. PL peak energy E_{peak} in sample C versus current density j at $T=5$ K for voltage-controlled (squares) as well as current-controlled (circles) measurements and versus sample temperature T (crosses) at zero bias. The horizontal scales have been adjusted relative to each other to clearly show the agreement of the effect of these two parameters.

be noted that, while the PL signal can be detected for current values above 0.6 kA cm^{-2} at 5 K, there is no PL signal at zero bias for temperatures above 60 K. The largest energy of the PL line occurs for a field strength of 44 kV cm^{-1}, which corresponds to the plateau of the *j-F* characteristic shown in Fig. 8.

IV. DISCUSSION

The carrier redistribution process between the active region and the injector is discussed using the coupling between subband states of coupled asymmetric QW's as outlined in Ref. 19. First, we consider the variation of the PL intensities of sample B as shown in Fig. 6. The horizontal lines 1–3 denote specific electric-field strengths, where the PL intensity exhibits characteristic changes, and the additional specific field strength denoted (4) was obtained from Fig. 7. The PL intensity depends on the distribution of both electrons and holes, and it has been shown that, for asymmetric double-quantum-well SL's, the dynamics of both electrons and holes also plays an important role for the variation of the PL intensity.[14,15] Therefore, it is necessary to distinguish between the contributions of electrons and holes. Since in the doped quasi-QCL structure of sample B′ the PL peak intensity for the wells 2 and 3 below point 2 does not significantly change, we can assume that the hole redistribution for sample B does not play an important role in this field region. In Fig. 6, the minima of the PL peak intensity for the wells 2 and 3 at point 1 suggest a redistribution of carriers between these wells. However, the PL peak intensity of well 1 does not change in this region. Therefore, we believe that this field strength aligns the subbands of wells 2 and 3. When this field strength is exceeded, the subband energy of well 2 becomes larger than that of wells 1 and 3 so that well 2 becomes depopulated. At larger electric fields, alignment between wells 1 and 3 should occur, which may happen at point 2. At this point, well 2 has been completely depopulated (the PL signal in Fig. 6 has disappeared), while the intensity of well 3 exhibits a maximum. The origin of point 3 is currently not clear, but it may be related to the interaction between well 1 and another state in the injector region, because the PL intensity of well 1 exhibits a minimum near this field strength. Point 4 corresponds to the field strength for miniband formation in the injector.

The carrier redistribution model as a function of the applied electric field is summarized in Fig. 11. The numbers in brackets correspond to the field ranges indicated in Fig. 6. The different panels describe the alignment of the levels in QW's 1, 2, and 3 as described above for sample B and below for sample A. Considering the carrier redistribution process discussed above, the coupling between the active and injector regions is probably important for the device function of the QCL. The barrier between the active and injector regions (the exit barrier) is the second thickest barrier in the entire QCL structure, and the overlap of the wave functions for the two wells on either side of this barrier should be rather weak. However, this barrier has two functions. It is necessary, first, to inhibit tunneling into higher energy states such as continuum states and, second, to ensure an efficient emptying of the ground state in the active region. Therefore, if the barrier becomes too thick, the carrier dynamics related to this barrier may become a bottleneck for the laser performance.

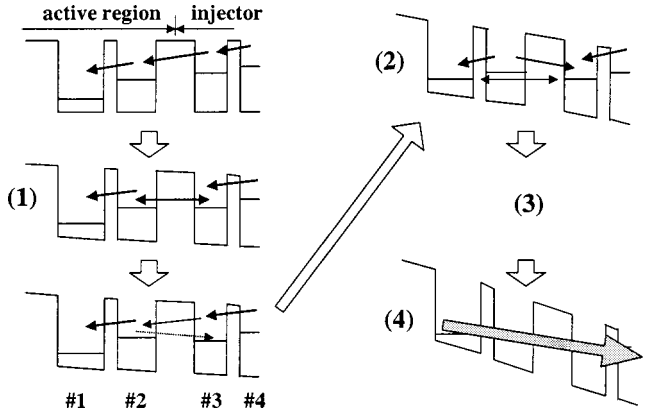

FIG. 11. Schematic diagrams for the carrier redistribution process in the quasi-QCL structure.

The miniband formation model shown in Fig. 11 can also be applied to the undoped QCL structure of sample A. The subband crossing between wells 1 and 3 is observed in Fig. 2 at point 2. By assuming an average electric field for the whole QCL structure, the energy level separation between the ground states of wells 1 and 3 can be approximated by a linear function, and the slope of this line is determined by the distance between the two wells. In this way, the black solid line from A_1 to A_2 in Fig. 2 can be inserted. Following this line, the ground state of well 3 is located about 37 meV above the ground state of well 1 at zero bias. With increasing electric field, the two ground states become aligned at about 28 kV cm^{-1} (point 2). At the field strength for miniband formation (point 4), the ground state of well 3 is at least 30 meV below the ground state of well 1.

In the same way, the level alignment between the ground states of wells 1 and 2 can be understood. The *j-F* characteristic of sample A in Fig. 4 shows characteristic features (two maxima and one jump) at points 2, 3, and 4, which are correlated with abrupt changes of the PL intensity in Fig. 2. These jumps are likely due to a resonance between the ground state in the widest well and the ground state of another well. As discussed above, the small jump at point 2 corresponds to the resonance between wells 1 and 3. The large jump at point 4, which occurs near the field strength for miniband formation in the injector, may also be related to a crossing of the ground states of wells 1 and 2, and the rather large change in the current suggests a strong coupling between these two states. Following the upper black line in Fig. 2, which shows the diagonal transition between wells 1 and 2, the ground states of wells 2 and 3 align at about 12 kV cm^{-1}, labeled as point 1. At zero bias, the ground state of well 2 is located about 26 meV above that of the widest well.

These results indicate that a phonon resonance between the ground states of wells 1 and 3 may play an important role for the operation of the laser. In this field region, the ground state of well 3 approaches an energy about 36 meV below that of the widest well, which corresponds to the optical phonon energy in GaAs. Therefore, it is expected that popu-

lation inversion may be enhanced by reducing the relaxation time for the transition from the ground state in well 1 to the ground state in well 3 via resonant phonon emission, similar to the double-phonon resonance proposed by Hofstetter *et al.*[20] The population inversion in the active region can therefore be directly influenced by the design of the injector and, in particular, of the corresponding exit barrier between the active region and the injector.

V. CONCLUSIONS

We have investigated the transport properties and carrier redistribution in QC structures. While the dark *j-F* characteristics of the undoped QCS (sample A) and quasi-QCS (sample B) exhibit only jumps or sharp peaks near the field strength for miniband formation in the injector, a plateau with a sawtoothlike structure is observed in the *j-F* characteristic of the complete QCL structure (sample C) below threshold. However, the illumination of samples A and B results only in a plateaulike structure in the corresponding *j-F* characteristic, which is probably related to an inhomogeneous field distribution within each period. The origin of both the plateaulike structure in samples A and B as well as the sawtoothlike structure in sample C requires further investigation. The PL spectra of the undoped QCS (sample A) as well as of the QCL structure (sample C) exhibit only one line originating from the widest QW. The PL lines from other wells may not be observable because of the fast hole relaxation into the widest QW due to the strong coupling between the QW's.

The quasi-QCS (sample B) enables the investigation and understanding of the carrier redistribution process as a function of the applied electric field. The corresponding processes can also be understood in the undoped QCS (sample A) with essentially the same description as for sample B. However, the doping of the layers in the injector for sample C strongly changes the carrier dynamics for electric fields below the formation of the miniband. A strong correlation between the specific features in the *j-F* characteristics below threshold, such as the plateau and the variation of the PL peak position, and the carrier distribution process is very probable.

ACKNOWLEDGMENT

This work was supported in part by the Deutsche Forschungsgemeinschaft within the framework of the Forschergruppe 394.

[1] J. Faist, F. Capasso, D. L. Sivco, C. Sirtori, A. L. Hutchinson, and A. Y. Cho, Science **264**, 553 (1994).
[2] M. Beck, D. Hofstetter, T. Aellen, J. Faist, U. Oesterle, M. Ilegems, E. Gini, and H. Melchior, Science **295**, 301 (2002).
[3] R. Köhler, A. Tredicucci, F. Beltram, H. E. Beere, E. H. Linfield, A. G. Davis, D. A. Ritchie, R. C. Iotti, and F. Rossi, Nature (London) **417**, 156 (2002).
[4] C. Gmachl, F. Capasso, D. L. Sivco, and A. Y. Cho, Rep. Prog. Phys. **64**, 1533 (2001).
[5] K. Ohtani and H. Ohno, Jpn. J. Appl. Phys., Part 2 **41**, L1279 (2002).
[6] L. R. Wilson, P. T. Keightley, J. W. Cockburn, J. P. Duck, M. S. Skolnick, J. C. Clark, G. Hill, M. Moran, and R. Grey, Appl. Phys. Lett. **75**, 2079 (1999).
[7] M. Giehler, R. Hey, H. Kostial, S. Cronenberg, T. Ohtsuka, L. Schrottke, and H. T. Grahn, Appl. Phys. Lett. **82**, 671 (2003).
[8] F. Eickemeyer, K. Reimann, M. Woerner, T. Elsaesser, S. Barbieri, C. Sirtori, G. Strasser, T. Müller, R. Bratschitsch, and K. Unterrainer, Phys. Rev. Lett. **89**, 047402 (2002).
[9] C. Sirtori, H. Page, C. Becker, and V. Ortiz, IEEE J. Quantum Electron. **38**, 547 (2002).
[10] S.-C. Lee and A. Wacker, Phys. Rev. B **66**, 245314 (2002).
[11] C. Sirtori, P. Kruck, S. Barbieri, P. Collot, J. Nagle, M. Beck, J. Faist, and U. Oesterle, Appl. Phys. Lett. **73**, 3486 (1998).
[12] H. T. Grahn, R. J. Haug, W. Müller, and K. Ploog, Phys. Rev. Lett. **67**, 1618 (1991).
[13] L. Schrottke, T. Ohtsuka, R. Hey, H. Kostial, and H. T. Grahn (unpublished).
[14] L. Schrottke, R. Hey, and H. T. Grahn, Appl. Phys. Lett. **79**, 629 (2001).
[15] L. Schrottke, R. Hey, H.-Y. Hao, T. Ohtsuka, and H. T. Grahn, Physica E (Amsterdam) **13**, 868 (2002).
[16] J. Ulrich, G. Strasser, and K. Unterrainer, Physica E (Amsterdam) **13**, 900 (2002).
[17] H. Onose, H. Yoshimura, and H. Sakaki, Appl. Phys. Lett. **54**, 2221 (1989).
[18] C. Cacciatore, D. Campi, C. Coriasso, C. Rigo, and C. Alibert, Phys. Rev. B **40**, 6446 (1989).
[19] J. E. Golub, P. F. Liao, D. J. Eilenberger, J. P. Harbison, L. T. Florez, and Y. Prior, Appl. Phys. Lett. **53**, 2584 (1988).
[20] D. Hofstetter, M. Beck, T. Aellen, and J. Faist, Appl. Phys. Lett. **78**, 396 (2001).